



20 **Abstract**

21 China has implemented some air pollution management measures in recent years, yet severe
22 ozone pollution remains a significant issue. The Southeastern Coast of China (SECC) is often
23 influenced by hot extremes and tropical cyclones (TCs), and the two can occur simultaneously (TC-
24 HDs). The compound TC-HDs show a rising trend in the summers of 2014—2019, potentially
25 affecting ozone pollution. Here, we found that surface ozone concentrations over SECC are elevated
26 during extreme hot days than the climatology. However, compared to extreme hot days alone
27 (AHDs), the maximum 8-hour average ozone (MDA8 O₃) concentration increases by an average of
28 6.8 µg/m³ in the Pearl River Delta (PRD) and decreases by 13.2 µg/m³ in the Yangtze River Delta
29 (YRD) during the compound TC-HDs. The meteorological conditions during AHDs favor the
30 chemical production of ozone over SECC, exhibiting increased temperature and solar radiation but
31 decreased relative humidity. Relative to AHDs, strong northeasterly winds prevail in SECC during
32 TC-HDs, suggesting the potential of ozone cross-regional transport between YRD and PRD. The
33 process analysis in the chemical transport model (GEOS-Chem) suggests that relative to AHDs, the
34 chemical production of ozone is enhanced in YRD during TC-HDs while horizontal transport
35 alleviates ozone pollution in YRD but worsens it in PRD through cross-regional transport. The
36 results highlight the significant effects of cross-regional transport in modulating ozone pollution in
37 the two megacity clusters during hot extremes accompanied by TC activities, giving insight into
38 future ozone control measures over SECC under global warming.

39



40 **1. Introduction**

41 Tropospheric ozone (O₃) is the predominant air pollutant in addition to fine particulate matter
42 (PM_{2.5}) in China (Fu et al., 2019), and it poses significant risks to human health and the ecosystem
43 (Feng et al., 2015; T. Wang et al., 2017). Long-term exposure to high concentrations of ozone could
44 lead to lung tissue damage and chronic obstructive pulmonary disease, thereby increasing premature
45 death (Turner et al., 2016; Liu et al., 2018). Chen et al. (2023) demonstrated that the deterioration
46 of ozone air quality is considered to be the primary factor responsible for the 90% increase in
47 premature respiratory mortalities in China from 2013 to 2019. Furthermore, ozone can negatively
48 impact crop yield by inhibiting plant photosynthesis, accelerating crop senescence, and reducing
49 both yield and quality (Ainsworth et al., 2012; Song and Hao, 2023), ultimately affecting ecosystem
50 stability (Gu et al., 2023).

51 To deal with the severe air pollution issues, China has implemented several pollution
52 prevention and control measures, which are prioritized to tackle the problem of particulate matter
53 (P. Wang et al., 2022), including the “Air Pollution Prevention and Control Action Plan” and the
54 “Three-Year Action Plan for Winning the Blue Sky Defense Battle”. As a result, these efforts are
55 making significant progress in lowering PM_{2.5} concentrations. Z. Wang et al. (2022) indicated that
56 the annual concentration of PM_{2.5} in China has decreased by 13.41 μg/m³ from 2014 to 2020.
57 However, it is worth noting that most cities in China still frequently experienced severe ozone
58 episodes (K. Li et al., 2019). It is demonstrated that surface ozone concentration in most regions of
59 China have increased by approximately 20% during the period from 2013 to 2017 (Huang et al.,
60 2018). Also, Wei et al. (2022) recently found that both surface ozone concentration and ozone



61 pollution (the maximum 8-hour average ozone (MDA8 O₃) concentrations exceed 160 µg/m³) days
62 in China exhibited an increasing trend from 2013 to 2020. Therefore, ozone pollution in China has
63 received widespread attention over the past few decades (Ashmore, 2005; Gong and Liao, 2019; N.
64 Wang et al., 2022).

65 Changes in tropospheric ozone are closely related to their precursor gases, including nitrogen
66 oxides (NO_x) and volatile organic compounds (VOCs) (Fu and Liao, 2014; Jacob et al., 1999; K. Li
67 et al., 2019). Zhang et al. (2023) revealed that an increase in biogenic volatile organic compounds
68 (BVOCs) increased local ozone production by 23% per year in Hong Kong. K. Li et al. (2019)
69 pointed out that anthropogenic NO_x emissions in China decreased by 21% from 2013 to 2017,
70 whereas VOCs emissions changed little. Decreasing NO_x would increase ozone under the VOC-
71 limited conditions prevailed in urban China but decrease ozone under rural NO_x-limited conditions.
72 In addition to precursor emissions, meteorological conditions can significantly modulate surface
73 ozone levels (Yin et al., 2019; Zhou et al., 2022). For example, severe ozone pollution commonly
74 occurs during summertime with high temperatures, low relative humidity (RH), and strong solar
75 radiation (Dai et al., 2023; Yin et al., 2019). Under low RH conditions, trees close the stomata
76 (pores for exchanging CO₂ and water vapor), inhibiting the dry deposition of ozone and leading to
77 ozone accumulation (Kavassalis and Murphy, 2017). Besides, low humidity conditions inhibit ozone
78 breakdown as the O(¹D) combines with water molecules (H₂O) to produce hydroxyl radicals that
79 promote ozone decomposition in high humidity environments (M. Li et al., 2021). Wind direction
80 and wind speed play an important role in the transport and diffusion of ozone (Banta et al., 2011;
81 Jammalamadaka and Lund, 2006). It is proved that the co-occurred heat waves and atmospheric



82 stagnation days with low wind speed favor ozone pollution in the U.S. through promoting the ozone
83 production (Zhang et al., 2018). Reduced clouds and strengthened solar radiation during the hot
84 extremes favor photochemical ozone production in the troposphere and thus increase the surface
85 ozone concentrations (P. Wang et al., 2022). Large-scale atmospheric circulation can modulate
86 surface ozone through changing the meteorological conditions (Yang et al., 2022). For instance, the
87 stronger western Pacific subtropical high (WPSH) leads to higher temperatures, stronger solar
88 radiation, lower RH, and less precipitation, which favors the production and accumulation of surface
89 ozone in northern China (Jiang et al., 2021).

90 Extreme weather events, especially heat waves and tropical cyclones (TCs), have a significant
91 impact on ozone in eastern China (Lin et al., 2019; T. Wang et al., 2017). High ozone concentration
92 events are typically associated with high temperatures, which lead to increased emissions of BVOCs
93 and enhance the chemical formation of ozone (Lu et al., 2019; P. Wang et al., 2022). TC activities
94 can substantially affect tropospheric ozone through affecting the transport, production and
95 accumulation processes over the coastal regions of China (K. Meng et al., 2022; Qu et al., 2021;
96 Zhan et al., 2022). For ozone pollution over the Yangtze River Delta (YRD) region, the peripheral
97 circulations of the approaching TCs intensify downward airflow, resulting in a short-term local
98 weather pattern of high temperatures, low humidity, intense solar radiation, and light winds,
99 exacerbate ozone pollution (Shu et al., 2016), and following the passage of TCs, the lower
100 tropospheric transport of ozone-rich air and strong photochemical reactions also amplify ozone
101 pollution (Zhan et al., 2020). For ozone pollution in Pearl River Delta (PRD), influenced by the
102 strong downdrafts related to the periphery of TCs, the PRD region typically is dominated by high



103 pressure, low humidity, and strong solar radiation, leading to the accumulation of ozone (Wei et al.,
104 2016; Ouyang et al., 2022). Moreover, TC activities are proven to enhance the chemical interactions
105 between anthropogenic and biogenic emissions, resulting in extreme ozone pollution over both the
106 YRD and PRD regions (N. Wang et al., 2022).

107 The southeastern coastal region of China (SECC), including the YRD and PRD regions,
108 experiences both frequent TCs and heatwave events under global warming (W. Wang et al., 2016;
109 Xiao et al., 2011). And there is a significant concurrent relationship between extreme heatwaves and
110 TC activity that the peripheral circulations of TCs can promote extreme heatwaves (P. Wang et al.,
111 2023; Zhang et al., 2024). Such compound hazards are more destructive than the individual extremes
112 (Matthews et al., 2019). The SECC region has experienced a considerable rise in surface ozone
113 concentrations during the period from 2013 to 2019 (X. Meng et al., 2022). Although the individual
114 effects of heatwaves and TCs on ozone have been emphasized, the effects of the compound extremes
115 of heat waves and TCs on ozone pollution have received limited attention.

116 In this study, we aim to investigate the impacts of the compound hazards of TCs and extreme
117 hot days (TC-HDs) on ozone pollution in SECC (105—125° E, 10—35° N) based on the long-term
118 (2014—2019) observational records of air temperatures and TCs, reanalysis datasets of ground-
119 level ozone concentrations and meteorological parameters, and the GEOS-Chem model simulations.
120 The mechanisms contributing to these impacts are also analyzed. The study is organized as follows:
121 Section 2 presents the methods and data utilized, and Section 3 describes the spatial and temporal
122 variations of TC-HDs observed in SECC during 2014—2019. Section 4 describes the impacts of
123 TC-HDs on ozone concentration in SECC, with a focus on YRD and PRD regions. In Section 5, we



124 investigate the possible mechanisms for the anomalous ozone concentrations in SECC during TC-
125 HDs as well as the differences between YRD and PRD by investigating the meteorological
126 conditions and key chemical and physical process analysis with the GEOS-Chem model. Finally,
127 Section 6 provides a summary and discussion.

128 **2. Data and methods**

129 **2.1 Observational datasets**

130 In this work, we focus on the ozone pollution over SECC where is vulnerable to both severe
131 hot extremes and ozone pollution (Ma et al., 2019; P. Wang et al., 2022). Moreover, population and
132 economic are prominent. The daily maximum air temperatures (T_{\max}) from more than 1400
133 observation sites in the domain for the period 2014—2019 are provided by the China Meteorological
134 Administration (CMA). The best track dataset of TCs is also released by CMA (accessible at [https://
135 tcdata.typhoon.org.cn/zjljsjj_sm.html](https://tcdata.typhoon.org.cn/zjljsjj_sm.html)). This dataset includes the time, location, and intensity of TCs,
136 which records all TCs that have passed through the western North Pacific (WNP) since 1949 (Lu et
137 al., 2021; Ying et al., 2014).

138 **2.2 Reanalysis datasets**

139 The ground-level ozone concentrations for the period 2014—2019 are obtained from the high-
140 resolution and high-quality ground-level MDA8 ozone data (unit: $\mu\text{g}/\text{m}^3$) for China (ChinaHighO₃)
141 at a resolution of $0.1^\circ \times 0.1^\circ$, which is one of the series of the high-resolution and high-quality
142 ground-level air pollutants in China (Wei et al., 2022). The ChinaHighO₃ dataset provides reliable
143 estimates of MDA8 ozone, demonstrated by an average out-of-sample (out-of-station) coefficient
144 of determination of 0.87 (0.80) and a root-mean-square error of 17.10 (21.10) $\mu\text{g}/\text{m}^3$ across China



145 (Wei et al., 2022).

146 Meteorological parameters including 2-meter air temperature (T2m), relative humidity (RH),
147 surface solar radiation downwards (SSRD), geopotential height (HGT), eastward wind (uwnd),
148 northward wind (vwnd), mean sea level pressure (MSLP) and total cloud cover (TCC) are from the
149 fifth generation of the European Centre for Medium-Range Weather Forecasts (ECMWF) reanalysis
150 data (ERA5), the latest global atmospheric reanalysis of ECMWF (Hersbach et al., 2020). The
151 temporal resolution for T2m, SSRD, and TCC is 6 hours, while that for other meteorological
152 parameters is 3 hours, which are all utilized to generate daily mean values.

153 **2.3 Identifications of extreme events**

154 Severe ozone pollution episodes generally occur in SECC during summertime, coinciding with
155 frequent heatwaves and TCs (Ji et al., et al., 2024; Shu et al., 2016). In this work, we focus on the
156 impacts of extreme high temperatures and TCs on surface ozone during summer only (June, July,
157 and August) in SECC, as outlined in Figure 2. P. Wang et al. (2022) pointed out that most TC tracks
158 over the western North Pacific passed through the SECC region during their lifetimes in the past
159 several decades. The hot days (HDs) are defined as dates when the number of observation stations
160 with a Tmax exceeding 35°C exceeds more than 40% of the total number of observation stations
161 within the SECC. We use the proportion of high-temperature sites exceeding 40% as a measure of
162 HDs to ensure adequate samples and extremely hot conditions over SECC during HDs. Note that
163 the anomalies of surface ozone concentrations show similar spatial patterns during HDs with a lower
164 (30%) or higher (50%) threshold for hot sites (not shown). In this work, we classify all HDs into
165 two categories: tropical cyclone-hot days (TC-HDs) and alone hot days (AHDs). TC-HDs are



166 identified when hot days occur over the land regions within SECC, concurrent with the passages of
167 tropical cyclones through the area; and AHDs indicate hot days that occur independently.

168 **2.4 GEOS-Chem model**

169 In this study, surface ozone concentrations during 2014—2019 are simulated by using the 3-D
170 global chemical transport model (GEOS-Chem, version 13.4.1) with a horizontal resolution of 2°
171 latitude × 2.5° longitude and 47 vertical layers from the surface to 0.01 hPa. The GEOS-Chem has
172 the fully coupled O₃–NO_x–hydrocarbon–aerosol chemical mechanisms (Pye et al., 2009; Sherwen
173 et al., 2016) used to simulate concentrations of gas-phase pollutants (such as ozone) and aerosols.
174 It is driven by assimilated meteorological data of version 2 of Modern-Era Retrospective analysis
175 for Research and Applications (MERRA2; Gelaro et al., 2017)

176 The anthropogenic emissions of ozone precursor gases, including CO, NO_x, and non-methane
177 volatile organic compounds (NMVOCs) are provided by the Community Emissions Data System
178 (CEDS) (Hoesly et al., 2018). Methane (CH₄) concentrations are provided by the Global Monitoring
179 Division (GMD) of the National Oceanic and Atmospheric Administration (NOAA). Biomass
180 burning emissions are obtained from the Global Fire Emissions Database version 4 (GFEDv4) (Van
181 Der Werf et al., 2017). The biogenic emissions are estimated with the Model of Emissions of Gases
182 and Aerosols from Nature (MEGAN) version 2.1 (Guenther et al., 2012). Our previous studies show
183 that GEOS-Chem model excels in accurately reproducing observed ozone concentrations and spatial
184 distributions in China (Yang et al., 2022, 2014).

185 Meteorological conditions can modulate surface ozone concentrations through affecting the
186 physical and chemical processes including chemical production, horizontal advection, vertical



187 advection, dry deposition and diffusion (Gong and Liao, 2019). In this work, we use quantify the
188 contributions of individual processes to ozone changes with the model outputs of GEOS-Chem
189 (Gong and Liao, 2019; Ni et al., 2024; Shu et al., 2016). In the GEOS-Chem model, the change in
190 ozone over time step are caused by chemical production, horizontal advection, vertical advection,
191 dry deposition and diffusion, which can be used for separating out and quantifying the contributions
192 of individual physical and chemical processes to the changes in the simulated ozone concentrations
193 (Gong and Liao, 2019; Ni et al., 2024; Shu et al., 2016).

194 **3. Spatial and temporal variations of compound TC-HDs**

195 There are 63 days of TC-HDs over SECC during the summers of 2014—2019, accounting for
196 around 70% of the total HDs (91 days), with 28 hot days (30%) occurring alone (AHDs) in the past
197 6 years. The monthly variations of HDs, TCs, and TC-HDs over SECC from 2014 to 2019 are
198 displayed in Figure 1. All the weather extremes show notable intraseasonal variations with relatively
199 higher occurrences in July and August but lower occurrences in June each year. Besides, both the
200 occurrences of HDs and TCs demonstrate significant upward trends at the 90% confidence level,
201 with a rate of 0.31 days per month and 0.33 days per month, respectively. TC-HDs also show an
202 increasing trend with a rate of increase of 0.2 days/month, consistent with the variations of HDs and
203 TCs in the past six years. Hence, it is essential to examine the effects of rising TC-HDs on ozone
204 pollution in the SECC region.

205 Figure 2 demonstrates the spatial features of TC-HDs during 2014—2019. China
206 Meteorological Administration classifies tropical cyclones into 6 classes based on their intensity,
207 namely Tropical Depression (TD, 10.8—17.1 m/s), Tropical Storm (TS, 17.2—24.4 m/s), Strong



208 Tropical Storm (STS, 24.5—32.6 m/s), Typhoon (TY, 32.7—41.4 m/s), Strong Typhoon (STY,
209 41.5—50.9 m/s) and Super Typhoon (SSTY, ≥ 51.0 m/s). TCs are generally stronger before their
210 landfalls, which can reach STY and even SSTY (Fig. 2a and 2c), consistent with previous findings
211 (Han et al., 2022; Tuleya et al., 1984). TCs that affect the SECC primarily originate east of 135° E
212 and move westward to the eastern coastal regions. Around 90% of TCs associated with TC-HDs
213 make landfalls while the others weaken and dissipate over the ocean. Moreover, the air temperatures
214 over land regions of SECC during the TC-HDs are generally high, where the average T_{\max} of most
215 sites are beyond 35°C and reach up to 38°C (Fig. 2a). Compared with the summer climatology from
216 2014 to 2019, the average T_{\max} during TC-HDs increased approximately 4°C over most land
217 regions of SECC (Fig. 2c).

218 The temporal variations of the proportion of high-temperature sites ($T_{\max} \geq 35^\circ\text{C}$) and the
219 temperature anomalies relative to the summertime climatology averaged for the SECC land regions
220 along with the movements of TCs are given in Figs. 2b and 2d. The two variables demonstrate
221 similar patterns of variation. As TCs approach land regions, both the high-temperature sites and
222 temperature anomalies are increasing gradually, with a particularly pronounced temperature
223 increase associated with TCs moving towards the PRD regions. In contrast, there is typically a
224 decline in both the average air temperatures and the proportion of high-temperature sites following
225 the landfalls of TCs, which could be related to the strong wind and rainfall associated with the TCs
226 (Gori et al., 2022).

227 **4. Influences of TC-HDs on surface ozone concentrations in SECC**



228 Extreme high temperatures and the accompanied meteorology such as high-pressure systems
229 and strong radiation can affect local ozone pollution by enhancing chemical production and/or
230 accumulation (Gong and Liao, 2019; P. Wang et al., 2022; X. Wang et al., 2009). It is also well
231 demonstrated that extreme high temperatures and TCs can affect the ozone pollution over coastal
232 regions of China (Ding et al., 2023; Huang et al., 2011; N. Wang et al., 2022). In this work, we
233 further focus on the impacts of TC-HDs on surface ozone concentrations over land regions of SECC.
234 Figure 3 presents the spatial distributions of ozone concentration anomalies during TC-HDs and
235 AHDs relative to the summertime climatology from 2014—2019, as well as the differences between
236 the two. Notable increases in surface ozone concentrations are observed over most land regions of
237 SECC during the AHDs period, with anomalous MDA8 ozone reaching $40 \mu\text{g}/\text{m}^3$ and $20 \mu\text{g}/\text{m}^3$
238 over the YRD ($118\text{--}122^\circ \text{E}$, $30\text{--}33^\circ \text{N}$) and PRD ($110\text{--}115.5^\circ \text{E}$, $21.5\text{--}24^\circ \text{N}$) regions, respectively
239 (Fig. 3a), consistent with previous finding that hot extremes can worsen ozone pollution (P. Wang
240 et al., 2022). During the compound TC-HDs, most land regions except Hainan Island and the
241 northern part to 33°N of SECC experience a significant enhancement in surface ozone
242 concentrations, with MDA8 ozone anomalies above $20 \mu\text{g}/\text{m}^3$ overall (Fig. 3b). Compared to AHDs,
243 ozone concentrations in the easternmost coastal regions of China including YRD (outlined in Fig.
244 3c) are suppressed while ozone concentrations over the southernmost coastal regions of China
245 including PRD (outlined in Fig. 3c) are promoted during the compound TC-HDs. Comparing to TCs
246 occurring alone, surface ozone concentrations over most land regions of SECC increase during TC-
247 HDs (Fig. S1), which should be attributed to the increases in air temperatures. In this work, we



248 deliberately investigate the enhanced surface ozone concentration of PRD and the contrasting
249 depression over YRD during the compound TC-HDs.

250 The temporal variations of anomalous MDA8 ozone in YRD and PRD regions relative to the
251 summertime climatology with TC tracks during TC-HDs are shown in Figure 4. Surface ozone
252 concentrations over YRD are abnormally higher when TCs are positioned a long distance from land
253 regions, whereas ozone concentrations fall dramatically when TCs approach and make landfall over
254 land regions. And it should be noted that the surface ozone concentrations are elevated by the TCs
255 moving westward YRD while most of the other TCs cause a decline in ozone concentrations with
256 their approach to land regions, consistent with previous work (Shu et al., 2016). Zhan et al. (2020)
257 revealed that O₃ pollution episodes in YRD mainly occurred when a TC is near the 24 h warning
258 line before it landed on the coastline of the YRD as the YRD was influenced by an inland wind
259 carrying a significant amount of precursor substances from polluted areas while the increased
260 precipitation and strong winds resulted in decreased ozone concentrations when the TC was close
261 enough. For PRD, surface ozone concentrations increase noticeably when TCs approaching land
262 regions. Particularly, the TCs heading northeast to YRD favor the increases in ozone concentrations
263 in the PRD whereas the others tend to cause a reduction in surface ozone concentrations following
264 landfalls.

265 **5. Possible mechanisms underlying the impacts of TC-HDs on surface ozone**

266 **5.1 The dominant synoptic circulations**

267 The synoptic meteorological conditions during AHDs and TC-HDs are analyzed to disentangle
268 the different responses of surface ozone to hot extremes superimposed by TCs. Specifically, we



269 examine the composites of daily mean air temperature at 2m (T2m), relative humidity (RH), surface
270 solar radiation downwards (SSRD), mean sea level surface (MSLP), geopotential height at 500 hPa
271 (500hPa HGT) and 10-meter wind speeds, and total cloud cover (TCC) anomalies relative to
272 summertime climatology from 2014 to 2019 during AHDs (Fig. 5) and TC-HDs (Fig. 6), as well as
273 the differences between the two periods (Fig. 7). During the AHDs period, the land regions of SECC
274 are covered by increased T2m, decreased RH, reduced TCC, and enhanced SSRD (Figs. 5a-d),
275 which are favorable for the chemical formation of ozone therein (Yin et al., 2019), supporting the
276 elevated surface ozone during AHDs as shown in Figure 3a. In the mid-upper troposphere, a band
277 of positive HGT at 500hPa (H500) anomalies dominate most land regions of China and extends
278 northeastward to Korea, with westerly wind anomalies in the northern flank and easterly wind
279 anomalies in the southern flank (Fig. 5f), indicating a westward extension and strengthening of the
280 western North Pacific subtropical high (WNPSH), favoring the occurrences of hot extremes over
281 southern China (Luo & Lau, 2017; P. Wang et al., 2018). Besides, it's noticed that negative H500
282 anomalies and cyclonic circulation appear over the east of 125° E which are also seen at the surface
283 (Fig. 5e) with anomalous southwesterly prevails over SECC land regions at the surface (Fig. 5e).
284 Such a low-pressure system characterizes TC track which finally recurve northeastward (Fig. S2).

285 During TC-HDs, the land regions of SECC are covered by increased T2m, decreased RH,
286 reduced TCC, and enhanced SSRD (Figs. 6a-d), favoring the enhanced chemical formation of ozone
287 therein, supporting the elevated surface ozone during TC-HDs as shown in Figure 3b. In the mid-
288 upper troposphere, positive H500 anomalies cover nearly the whole land region of China with
289 maximum dominating Korea, accompanied by anomalous anticyclonic circulation. Such changes



290 characterize the strengthening and westward extension of WPSH (Fig. 6f), favoring more hot
291 extremes. A dipole pattern of MSLP anomalies can be observed at the surface, with an abnormal
292 low-pressure center over the South China Sea and another to its east (Fig. 6e). Besides, the land
293 regions are influenced by weak winds at the surface (Fig. 6e).

294 Figure 7 demonstrates the differences in meteorological variables between the periods of TC-
295 HDs and AHDs. Compared to AHDs, the YRD experiences an increase in T2m of approximately
296 1°C, while the PRD experiences a decrease in T2m of around 0.5°C during TC-HDs. In the
297 meanwhile, RH and TCC values are increased (decreased) in PRD (YRD) while SSRD values are
298 decreased (increased) in PRD (YRD) (Figs. 7a-d). The large-scale circulations in the middle-upper
299 troposphere show positive H500 anomalies over the north and northeast parts of China including
300 YRD while southern China including PRD is dominated by negative H500 anomalies, supporting
301 the increased T2m (decreased) over YRD (PRD). Moreover, a cyclonic circulation controls southern
302 China with YRD influenced by strong southeasterly winds while PRD is influenced by inland
303 northeasterly winds (Fig. 7f). The changes in MSLP show a similar pattern to H500 anomalies with
304 positive anomalies over YRD but negative anomalies over PRD, and an anomalous low-pressure
305 system is observed over South China Sea, accompanied by strong cyclonic circulation at the surface.
306 It should be noted that the YRD is influenced by strong easterly winds from the ocean and the clean
307 winds may alleviate ozone pollution as shown in Figure 3c. In contrast, PRD is influenced by strong
308 northeasterly winds from inland which is opposite to the climatological southwesterlies of the
309 summer monsoon circulation, which may favor the accumulation of ozone pollution therein, as
310 shown in Fig. 3c



311 It should be noted that the meteorological conditions in YRD favor the chemical production of
312 ozone yet reduced ozone concentrations are observed in YRD during TC-HDs relative to AHDs.
313 The key physiochemical processes associated with the alleviated ozone pollution over YRD but
314 worsened ozone pollution over PRD during TC-HDs relative to AHDs are explored with GEOS-
315 Chem model simulations in the following part.

316 **5.2 Process analysis with GEOS-Chem model simulations**

317 In this section, process analysis is conducted in the GEOS-Chem model to quantify the
318 contributions of each process, including net chemical production, horizontal advection, vertical
319 advection, and mixing (diffusion and dry deposition) to the anomalous surface ozone concentrations
320 over PRD and YRD during TC-HDs, respectively. The observed and simulated anomalous surface
321 MDA8 ozone during TC-HDs relative to the summer climatology mean and AHDs are given in
322 Figure S3 and the regional averages of surface MDA8 ozone concentrations over YRD and PRD
323 are summarized in Table 1. GEOS-Chem simulation can reasonably capture the spatial pattern of
324 anomalous surface MDA8 ozone concentrations during TC-HDs relative to the summer climatology
325 mean (Figs. S3a and b), and relative to AHDs (Figs. S3c and d). Particularly, compared to AHDs,
326 the simulated surface MDA8 ozone concentrations are inhibited over YRD but enhanced over PRD
327 during TC-HDs. As listed in Table 1, compared to AHDs, during TC-HDs, the observed (simulated)
328 average surface MDA8 ozone concentrations in the YRD decreased by $13.21 \mu\text{g}/\text{m}^3$ ($21.94 \mu\text{g}/\text{m}^3$),
329 whereas it increased by $6.8 \mu\text{g}/\text{m}^3$ ($7 \mu\text{g}/\text{m}^3$) in the PRD. This suggests that the model simulation
330 can reasonably capture the opposite changes in surface MDA8 ozone concentrations over the YRD
331 and PRD during extreme HDs superimposed by TCs.



332 Figure 8 illustrates the vertical profiles of simulated daily mean ozone concentrations for YRD
333 and PRD from surface to 500 hPa for the summer climatology, TC-HDs and AHDs during 2014—
334 2019, respectively. For YRD, surface ozone concentrations are apparently higher during AHDs than
335 those during TC-HDs and summertime climatology from surface up to the 500 hPa level (Fig. 8a).
336 This indicates that the enhancements in ozone concentrations during AHDs occur not only at the
337 surface but also to the middle of the troposphere. In addition, compared with the summertime
338 climatology, ozone concentrations in YRD during TC-HDs are slightly enhanced from surface to
339 850 hPa as well as between 600 hPa and 500 hPa while suppressed between 850hPa and 600 hPa.
340 For the PRD, ozone concentrations during TC-HDs are higher than the summertime mean and AHDs
341 from the surface up to 500 hPa (Fig. 8b). The ozone concentrations during AHDs are comparable to
342 (slightly stronger than) the summertime mean below (above) 850 hPa (Fig. 8b) based on the GEOS-
343 Chem model simulation.

344 We further analyze the main physiochemical processes affecting ozone concentration,
345 including net chemical production, vertical advection, horizontal advection and mixing (the sum of
346 dry deposition and diffusion). Figures 9 and 10 show the vertical profiles of the anomaly of each
347 process during TC-HDs and AHDs, relative to the summertime climatology over the YRD and PRD,
348 as well as the differences between TC-HDs and AHDs. During AHDs, the increase in ozone
349 concentrations in the YRD from the surface to 900 hPa is primarily contributed by chemical
350 production, while transport processes tend to decrease ozone concentration. Between 900 hPa and
351 700 hPa, the mixing process contributes to the increases in ozone concentrations while the transport
352 processes and chemical productions tend to decrease ozone concentrations. Between 700 hPa and



353 500 hPa, horizontal transport hampers ozone increase, while chemical production and vertical
354 transport contribute to ozone enhancement (Fig. 9a). During TC-HDs, the horizontal transport
355 exhibits a suppressive effect on ozone concentrations in the YRD from the surface up to 500 hPa
356 whereas the chemical production contributes to increases in ozone concentration. And two processes
357 overtake the effects of vertical transport and mixing (Fig. 9b). In comparison with AHDs, during
358 TC-HDs, ozone concentration increases due to chemical production exceed decreases caused by
359 horizontal transport between the surface and 850 hPa. However, between 850 hPa and 700 hPa, the
360 decrease in ozone concentration due to horizontal transport outweighs the increase from chemical
361 production. Overall, compared to AHDs, the chemical production contributes to increased ozone
362 concentrations in the YRD from the surface up to 500 hPa during TC-HDs, whereas the horizontal
363 transport tends to lower ozone concentrations. As listed in Table 2, compared to AHDs, ozone
364 chemical production plays a predominant role in enhancing ozone pollution during TC-HDs in the
365 YRD (1.24 Gg O₃/day), whereas horizontal transport significantly depresses ozone concentration
366 (−1.15 Gg O₃/day). As stressed above, the strong and clean oceanic winds along YRD can help
367 alleviate ozone pollution. The vertical transport and mixing processes play a less important role in
368 affecting ozone concentrations in YRD during TC-HDs.

369 For PRD, the horizontal transport primarily contributes to decreased ozone concentrations in
370 the PRD between the surface and 500 hPa during AHDs. The chemical production, vertical transport
371 and mixing processes exhibit promoting effects on ozone concentrations from surface to 700 hPa
372 (Fig. 10a). During TC-HDs, horizontal transport predominantly contributes to increased ozone
373 concentrations over PRD from surface to 900 hPa and between 850 hPa and 500 hPa and the



374 chemical production increases ozone concentrations between 950 hPa and 800 hPa. In contrast, the
375 mixing process and vertical transport play a dominant role in reducing ozone concentrations
376 between the surface to 900 hPa and between 900 hPa to 500 hPa respectively (Fig. 10b). Compared
377 to AHDs, during TC-HDs, transport processes predominantly contribute to the increases in ozone
378 concentrations in the PRD from the surface up to 500 hPa. Additionally, between 900 hPa and 800
379 hPa, chemical production plays a positive role in enhancing ozone concentrations. As listed in Table
380 3, during TC-HDs compared to AHDs, the horizontal transport process in the PRD exhibits a
381 significantly stronger enhancing effect on ozone concentrations from surface to 500 hPa (1.81 Gg
382 O₃/day) compared to the other three processes. Note that the summer climatology of ozone
383 concentrations in YRD is significantly higher than that in PRD (Fig. S4) and the cross-section of
384 wind anomalies demonstrates that strong winds from YRD to PRD exist during TC-HDs (Fig. S5),
385 implying strong ozone mass transport from YRD to PRD. Thus, the cross-region transport may play
386 a significant role in worsening ozone pollution over RPD during TC-HDs relative to AHDs.

387 In summary, favorable synoptic patterns during extreme hot days promote the chemical
388 production of ozone, and thus exacerbate ozone pollution over both YRD and PRD. Compared to
389 AHDs, the anomalously meteorological conditions during TC-HDs, enhance the chemical
390 production of ozone in the YRD while the horizontal transport process mitigates ozone pollution
391 therein but worsens ozone pollution in PRD through cross-regional transport, finally resulting in an
392 increase in ozone in PRD but a decrease in YRD.

393 **6. Conclusion and discussions**

394 China has implemented a series of emission reduction strategies to alleviate air pollution, and



395 $PM_{2.5}$ concentrations have decreased significantly while ozone pollution remains a major concern.
396 Ozone pollution is sensitive to meteorological conditions, especially the extreme weathers that
397 frequently strike China under global warming. Eastern China is economically developed and
398 densely populated, with serious ozone pollution. It is also vulnerable to both extreme hot weathers
399 and TCs during the summer. In this work, we deliberately investigate the impacts of extreme hot
400 weathers on surface ozone for the summers of 2014—2019 over SECC coupled with (TC-HDs) and
401 without TCs (AHDs) over the ocean. The associated synoptic conditions and physicochemical
402 processes are assessed combined reanalysis dataset with the GEOS-Chem model simulations.

403 Results show that the surface ozone concentrations over most land regions within SECC are
404 elevated during both TC-HDs and AHDs relative to the climatological mean, however, there are
405 considerable differences between the two events. Compared to AHDs, the surface ozone
406 concentrations are noticeably decreased in the YRD region but increased in the PRD region during
407 TC-HDs periods. The meteorological conditions suggest that though YRD is influenced by higher
408 temperature, lower humidity, and stronger radiation during TC-HDs than AHDs, it is influenced by
409 strong and clean sea winds, which aid in ozone elimination. In contrast, the PRD is influenced by
410 the strong northeasterly winds, opposite to the climatology, and may transport ozone pollution from
411 polluted regions. Such a hypothesis is validated with the GEOS-Chem simulation. Compared with
412 AHDs, among all the physicochemical processes, horizontal transport plays a crucial role in
413 increasing (reducing) ozone levels over PRD (YRD). Compared to AHDs, the horizontal transport
414 contributes to -1.15 Gg O_3 /day and 1.8 Gg O_3 /day to the net changes in tropospheric ozone mass
415 from surface to 500 hPa in YRD and PRD during TC-HDs. The findings will provide significant



416 implications for the control measures of ozone pollution in PRD and YRD during hot extremes, to
417 consider the significant impacts of TC activities.

418 Extreme hot weathers are projected to be more frequent and intensified in the future under the
419 continued global warming (P. Wang et al., 2019). Moreover, it is projected that TCs and heatwave
420 compound events are projected to significantly increase in their intensity and frequency over the
421 Northwest Pacific, causing potentially enlarged population exposures for the southeastern coast of
422 China (Wu et al. 2022). Therefore, the potential impacts of extreme hot weather and the TC-HDs
423 on surface ozone over China warrants future efforts. BVOCs are important precursors of ozone, and
424 their emissions are greatly influenced by weather conditions. As revealed by N. Wang et al. (2022),
425 the TCs over Northwest Pacific could intensify the chemical interactions between anthropogenic
426 and biogenic emissions, resulting in extreme ozone pollution over YRD and PRD regions. The
427 responses of biogenic emissions during hot extremes accompanied by TCs deserve further
428 investigation.

429

430 **Data availability**

431 The ground-level ozone concentrations are obtained from the high-resolution and high-quality
432 ground-level daily maximum 8-hour average ozone (MDA8 O₃) data for China (ChinaHighO₃,
433 <https://doi.org/10.5281/zenodo.4400043>). Daily maximum air temperature is provided by the
434 National Meteorological Information Center of the China Meteorological Administration (CMA,
435 <http://data.cma.cn/en/>). The best track dataset of tropical cyclones is also released by CMA ([https://](https://tcdata.typhoon.org.cn/zjljsjj_sm.html)
436 tcdata.typhoon.org.cn/zjljsjj_sm.html). Meteorological conditions data are derived from the fifth



437 generation of ECMWF reanalysis data (ERA5, <https://cds.climate.copernicus.eu/>). The GEOS-

438 Chem model is available at <http://acmg.seas.harvard.edu/geos/>.

439 **Author contributions**

440 C. Qi performed the analyses and wrote the initial draft. P. Wang and Y. Yang conceived and

441 supervised the study. H. Li performed the GEOS-Chem simulations. P. Wang reviewed and edited

442 the initial draft. All the authors discussed the results and contributed to the final manuscript.

443 **Competing interests**

444 The authors declare that they have no competing interest.

445 **Acknowledgements**

446 This research was supported by the National Natural Science Foundation of China (grant

447 42293323, 42105166, and 41975159), the National Key Research and Development Program of

448 China (grant 2020YFA0607803 and 2019YFA0606800), Jiangsu Science Fund for Distinguished

449 Young Scholars (grant BK20211541, Y.Y.), and the Jiangsu Science Fund for Carbon Neutrality

450 (grant BK20220031, H.L.).

451



452 **References**

- 453 Ainsworth, E.A., Yendrek, C.R., Sitch, S., Collins, W.J., Emberson, L.D.: The Effects of
454 Tropospheric Ozone on Net Primary Productivity and Implications for Climate Change, *Annu.*
455 *Rev. Plant Biol.*, 63, 637–661, <https://doi.org/10.1146/annurev-arplant-042110-103829>, 2012.
- 456 Ashmore, M.R.: Assessing the future global impacts of ozone on vegetation, *Plant Cell Environ.*,
457 28, 949–964, <https://doi.org/10.1111/j.1365-3040.2005.01341.x>, 2005.
- 458 Banta, R.M., Senff, C.J., Alvarez, R.J., Langford, A.O., Parrish, D.D., Trainer, M.K., Darby, L.S.,
459 Michael Hardesty, R., Lambeth, B., Andrew Neuman, J.: Dependence of daily peak O₃
460 concentrations near Houston, Texas on environmental factors: Wind speed, temperature, and
461 boundary-layer depth, *Atmos. Environ.*, 45, 162–173,
462 <https://doi.org/10.1016/j.atmosenv.2010.09.030>, 2011.
- 463 Chen, L., Liao, H., Zhu, J., Li, K., Bai, Y., Yue, X., Yang, Y., Hu, J., Zhang, M.: Increases in ozone-
464 related mortality in China over 2013–2030 attributed to historical ozone deterioration and
465 future population aging, *Sci. Total Environ.*, 858, 159972,
466 <https://doi.org/10.1016/j.scitotenv.2022.159972>, 2023.
- 467 Dai, H., Huang, G., Wang, J., Zeng, H.: VAR-tree model based spatio-temporal characterization and
468 prediction of O₃ concentration in China, *Ecotoxicol. Environ. Saf.*, 257, 114960,
469 <https://doi.org/10.1016/j.ecoenv.2023.114960>, 2023.
- 470 Ding, H., Kong, L., You, Y., Mao, J., Chen, W., Chen, D., ... & Wang, X.: Effects of tropical cyclones
471 with different tracks on ozone pollution over the Pearl River Delta region, *Atmos. Res.*, 286,
472 106680, <https://doi.org/10.1016/j.atmosres.2023.106680>, 2023



- 473 Feng, Z., Hu, E., Wang, X., Jiang, L., Liu, X.: Ground-level O₃ pollution and its impacts on food
474 crops in China: A review, *Environ. Pollut.*, 199, 42–48,
475 <https://doi.org/10.1016/j.envpol.2015.01.016>, 2015.
- 476 Fu, Y., Liao, H.: Impacts of land use and land cover changes on biogenic emissions of volatile
477 organic compounds in China from the late 1980s to the mid-2000s: implications for
478 tropospheric ozone and secondary organic aerosol, *Tellus B Chem. Phys. Meteorol.*, 66, 24987,
479 <https://doi.org/10.3402/tellusb.v66.24987>, 2014.
- 480 Fu, Y., Liao, H., Yang, Y.: Interannual and Decadal Changes in Tropospheric Ozone in China and
481 the Associated Chemistry-Climate Interactions: A Review, *Adv. Atmospheric Sci.*, 36, 975–
482 993, <https://doi.org/10.1007/s00376-019-8216-9>, 2019.
- 483 Gelaro, R., McCarty, W., Suárez, M. J., Todling, R., Molod, A., Takacs, L., Randles, C. A.,
484 Darmenov, A., Bosilovich, M. G., Reichle, R., Wargan, K., Coy, L., Cullather, R., Draper, C.,
485 Akella, S., Buchard, V., Conaty, A., Da Silva, A. M., Gu, W., ... Zhao, B.: The Modern-Era
486 Retrospective Analysis for Research and Applications, Version 2 (MERRA-2), *J. Climate*, 30,
487 5419–5454, <https://doi.org/10.1175/JCLI-D-16-0758.1>, 2017.
- 488 Gong, C., Liao, H.: A typical weather pattern for ozone pollution events in North China,
489 *Atmospheric Chem. Phys.*, 19, 13725–13740, <https://doi.org/10.5194/acp-19-13725-2019>,
490 2019.
- 491 Gori, A., Lin, N., Xi, D., & Emanuel, K.: Tropical cyclone climatology change greatly exacerbates
492 US extreme rainfall–surge hazard, *Nat. Clim. Chang.*, 12, 171–178,
493 <https://doi.org/10.1038/s41558-021-01272-7>, 2022.



- 494 Gu, X., Wang, T., Li, C.: Elevated ozone decreases the multifunctionality of belowground
495 ecosystems, *Glob. Change Biol.*, 29, 890–908, <https://doi.org/10.1111/gcb.16507>, 2023.
- 496 Guenther, A.B., Jiang, X., Heald, C.L., Sakulyanontvittaya, T., Duhl, T., Emmons, L.K., Wang, X.:
497 The Model of Emissions of Gases and Aerosols from Nature version 2.1 (MEGAN2.1): an
498 extended and updated framework for modeling biogenic emissions, *Geosci. Model Dev.*, 5,
499 1471–1492, <https://doi.org/10.5194/gmd-5-1471-2012>, 2012.
- 500 Han, W., Wang, Y., & Liu, L.: The relationship between pre-landfall intensity change and post-
501 landfall weakening of tropical cyclones over China, *Front. Earth Sci.*, 10, 1082181,
502 <https://doi.org/10.3389/feart.2022.1082181>, 2022.
- 503 H. Hersbach, B. Bell, P. Berrisford, S. Hirahara, A. Horányi, J. Muñoz-Sabater, J. Nicolas, C. Peubey,
504 R. Radu, D. Schepers, A. Simmons, C. Soci, S. Abdalla, X. Abellan, G. Balsamo, P. Bechtold,
505 G. Biavati, J. Bidlot, M. Bonavita, G. de Chiara, P. Dahlgren, D. Dee, M. Diamantakis, R.
506 Dragani, J. Flemming, R. Forbes, M. Fuentes, A. Geer, L. Haimberger, S. Healy, R. J. Hogan,
507 E. Hólm, M. Janisková, S. Keeley, P. Laloyaux, P. Lopez, C. Lupu, G. Radnoti, P. de Rosnay,
508 I. Rozum, F. Vamborg, S. Villaume, J. N. Thépaut,: The ERA5 global reanalysis, *Q. J. R.*
509 *Meteorol. Soc.*, 146(730), 1999-2049, <https://doi.org/10.1002/qj.3803>, 2020.
- 510 Hoesly, R.M., Smith, S.J., Feng, L., Klimont, Z., Janssens-Maenhout, G., Pitkanen, T., Seibert, J.J.,
511 Vu, L., Andres, R.J., Bolt, R.M., Bond, T.C., Dawidowski, L., Kholod, N., Kurokawa, J., Li,
512 M., Liu, L., Lu, Z., Moura, M.C.P., O'Rourke, P.R., Zhang, Q.: Historical (1750–2014)
513 anthropogenic emissions of reactive gases and aerosols from the Community Emissions Data
514 System (CEDS), *Geosci. Model Dev.*, 11, 369–408, <https://doi.org/10.5194/gmd-11-369-2018>,



- 515 2018.
- 516 Huang, C., Chen, C. H., Li, L., Cheng, Z., Wang, H. L., Huang, H. Y., Streets, D. G., Wang, Y. J.,
517 Zhang, G. F., and Chen, Y. R.: Emission inventory of anthropogenic air pollutants and VOC
518 species in the Yangtze River Delta region, China, *Atmos. Chem. Phys.*, 11, 4105–4120,
519 <https://doi.org/10.5194/acp-11-4105-2011>, 2011.
- 520 Huang, J., Pan, X., Guo, X., Li, G.: Health impact of China's Air Pollution Prevention and Control
521 Action Plan: an analysis of national air quality monitoring and mortality data, *Lancet Planet.
522 Health*, 2, e313–e323, [https://doi.org/10.1016/S2542-5196\(18\)30141-4](https://doi.org/10.1016/S2542-5196(18)30141-4), 2018.
- 523 Jacob, D.J., Logan, J.A., Murti, P.P.: Effect of rising Asian emissions on surface ozone in the United
524 States, *Geophys. Res. Lett.*, 26, 2175–2178, <https://doi.org/10.1029/1999GL900450>, 1999.
- 525 Jammalamadaka, S.R., Lund, U.J.: The effect of wind direction on ozone levels: a case study,
526 *Environ. Ecol. Stat.*, 13, 287–298, <https://doi.org/10.1007/s10651-004-0012-7>, 2006.
- 527 Ji, X., Chen, G., Chen, J., Xu, L., Lin, Z., Zhang, K., Fan, X., Li, M., Zhang, F., Wang, H., Huang,
528 Z., & Hong, Y.: Meteorological impacts on the unexpected ozone pollution in coastal cities of
529 China during the unprecedented hot summer of 2022, *Sci. Total Environ.*, 914, 170035,
530 <https://doi.org/10.1016/j.scitotenv.2024.170035>, 2024.
- 531 Jiang, Z., Li, J., Lu, X., Gong, C., Zhang, L., Liao, H.: Impact of western Pacific subtropical high
532 on ozone pollution over eastern China, *Atmospheric Chem. Phys.*, 21, 2601–2613,
533 <https://doi.org/10.5194/acp-21-2601-2021>, 2021.
- 534 Kavassalis, S.C., Murphy, J.G.: Understanding ozone-meteorology correlations: A role for dry
535 deposition, *Geophys. Res. Lett.*, 44, 2922–2931, <https://doi.org/10.1002/2016GL071791>, 2017.



- 536 Li, K., Jacob, D.J., Liao, H., Shen, L., Zhang, Q., Bates, K.H.: Anthropogenic drivers of 2013–2017
537 trends in summer surface ozone in China, *Proc. Natl. Acad. Sci.*, 116, 422–427,
538 <https://doi.org/10.1073/pnas.1812168116>, 2019.
- 539 Li, M., Yu, S., Chen, X., Li, Z., Zhang, Y., Wang, L., Liu, W., Li, P., Lichtfouse, E., Rosenfeld, D.,
540 and Seinfeld, J. H.: Large scale control of surface ozone by relative humidity observed during
541 warm seasons in China, *Environ. Chem. Lett.*, 19, 3981–3989, [https://doi.org/10.1007/s10311-](https://doi.org/10.1007/s10311-021-01265-0)
542 [021-01265-0](https://doi.org/10.1007/s10311-021-01265-0), 2021.
- 543 Lin, X., Yuan, Z., Yang, L., Luo, H., Li, W.: Impact of Extreme Meteorological Events on Ozone in
544 the Pearl River Delta, China, *Aerosol Air Qual. Res.*, 19, 1307–1324,
545 <https://doi.org/10.4209/aaqr.2019.01.0027>, 2019.
- 546 Liu, H., Liu, S., Xue, B., Lv, Z., Meng, Z., Yang, X., Xue, T., Yu, Q., He, K.: Ground-level ozone
547 pollution and its health impacts in China, *Atmos. Environ.*, 173, 223–230,
548 <https://doi.org/10.1016/j.atmosenv.2017.11.014>, 2018.
- 549 Lu, X., Yu, H., Ying, M., Zhao, B., Zhang, S., Lin, L., Bai, L., Wan, R.: Western North Pacific
550 Tropical Cyclone Database Created by the China Meteorological Administration, *Adv.*
551 *Atmospheric Sci.*, 38, 690–699, <https://doi.org/10.1007/s00376-020-0211-7>, 2021.
- 552 Lu, X., Zhang, L., Chen, Y., Zhou, M., Zheng, B., Li, K., Liu, Y., Lin, J., Fu, T.-M., Zhang, Q.:
553 Exploring 2016–2017 surface ozone pollution over China: source contributions and
554 meteorological influences, *Atmospheric Chem. Phys.*, 19, 8339–8361,
555 <https://doi.org/10.5194/acp-19-8339-2019>, 2019.
- 556 Luo, M., & Lau, N.-C.: Heat Waves in Southern China: Synoptic Behavior, Long-Term Change, and



- 557 Urbanization Effects, *J. Climate*, 30(2), 703–720, <https://doi.org/10.1175/JCLI-D-16-0269.1>,
- 558 2017.
- 559 Ma, M., Gao, Y., Wang, Y., Zhang, S., Leung, L.R., Liu, C., Wang, S., Zhao, B., Chang, X., Su, H.,
- 560 Zhang, T., Sheng, L., Yao, X., Gao, H.: Substantial ozone enhancement over the North China
- 561 Plain from increased biogenic emissions due to heat waves and land cover in summer 2017,
- 562 *Atmos Chem Phys.*, 19, 12195–12207, <https://doi.org/10.5194/acp-19-12195-2019>, 2019.
- 563 Matthews, T., Wilby, R.L., Murphy, C.: An emerging tropical cyclone–deadly heat compound hazard,
- 564 *Nat. Clim. Change*, 9, 602–606, <https://doi.org/10.1038/s41558-019-0525-6>, 2019.
- 565 Meng, K., Zhao, T., Xu, X., Hu, Y., Zhao, Yang, Zhang, L., Pang, Y., Ma, X., Bai, Y., Zhao, Yuguang,
- 566 Zhen, S.: Anomalous surface O₃ changes in North China Plain during the northwestward
- 567 movement of a landing typhoon, *Sci. Total Environ.*, 820, 153196,
- 568 <https://doi.org/10.1016/j.scitotenv.2022.153196>, 2022.
- 569 Meng, X., Wang, W., Shi, S., Zhu, S., Wang, P., Chen, R., Xiao, Q., Xue, T., Geng, G., Zhang, Q.,
- 570 Kan, H., Zhang, H.: Evaluating the spatiotemporal ozone characteristics with high-resolution
- 571 predictions in mainland China, 2013–2019, *Environ. Pollut.*, 299, 118865,
- 572 <https://doi.org/10.1016/j.envpol.2022.118865>, 2022.
- 573 Ni, Y., Yang, Y., Wang, H., Li, H., Li, M., Wang, P.: Contrasting changes in ozone during 2019–2021
- 574 between eastern China and the other regions of China, *Sci. Total Environ.*, 908, 168272,
- 575 <http://dx.doi.org/10.2139/ssrn.4563723>, 2024.
- 576 Ouyang, S., Deng, T., Liu, R., Chen, J., He, G., Leung, J.C.H., Wang, N., Liu, S.C.: Impact of a
- 577 subtropical high and a typhoon on a severe ozone pollution episode in the Pearl River Delta,



- 578 China, *Atmospheric Chem. Phys.*, 22(16), 10751-10767, [https://doi.org/10.5194/acp-22-](https://doi.org/10.5194/acp-22-10751-2022)
579 [10751-2022](https://doi.org/10.5194/acp-22-10751-2022), 2022.
- 580 Pye, H.O.T., Liao, H., Wu, S., Mickley, L.J., Jacob, D.J., Henze, D.K., Seinfeld, J.H.: Effect of
581 changes in climate and emissions on future sulfate-nitrate-ammonium aerosol levels in the
582 United States, *J. Geophys. Res. Atmospheres*, 114, 2008JD010701,
583 <https://doi.org/10.1029/2008JD010701>, 2009.
- 584 Qu, K., Wang, X., Yan, Y., Shen, J., Xiao, T., Dong, H., Zeng, L., Zhang, Y.: A comparative study to
585 reveal the influence of typhoons on the transport, production and accumulation of O₃ in the
586 Pearl River Delta, *Atmospheric Chem. Phys.*, 21, 11593–11612, [https://doi.org/10.5194/acp-](https://doi.org/10.5194/acp-21-11593-2021)
587 [21-11593-2021](https://doi.org/10.5194/acp-21-11593-2021), 2021.
- 588 Sherwen, T., Schmidt, J.A., Evans, M.J., Carpenter, L.J., Großmann, K., Eastham, S.D., Jacob, D.J.,
589 Dix, B., Koenig, T.K., Sinreich, R., Ortega, I., Volkamer, R., Saiz-Lopez, A., Prados-Roman,
590 C., Mahajan, A.S., Ordóñez, C.: Global impacts of tropospheric halogens (Cl, Br, I) on oxidants
591 and composition in GEOS-Chem, *Atmospheric Chem. Phys.*, 16, 12239–12271,
592 <https://doi.org/10.5194/acp-16-12239-2016>, 2016.
- 593 Shu, L., Xie, M., Wang, T., Gao, D., Chen, P., Han, Y., Li, S., Zhuang, B., Li, M.: Integrated studies
594 of a regional ozone pollution synthetically affected by subtropical high and typhoon system in
595 the Yangtze River Delta region, China, *Atmospheric Chem. Phys.*, 16, 15801–15819,
596 <https://doi.org/10.5194/acp-16-15801-2016>, 2016.
- 597 Song, X., Hao, Y.: An assessment of O₃-related health risks and economic losses in typical regions
598 of China, *Front. Public Health*, 11, 1194340, <https://doi.org/10.3389/fpubh.2023.1194340>,



- 599 2023.
- 600 Tuleya, R. E., Bender, M. A., and Kurihara, Y.: A Simulation Study of the Landfall of Tropical
601 Cyclones, *Mon. Wea. Rev.*, 112, 124–136, [https://doi.org/10.1175/1520-0493\(1984\)112<0124:ASSOTL>2.0.CO;2](https://doi.org/10.1175/1520-0493(1984)112<0124:ASSOTL>2.0.CO;2), 1984.
- 603 Turner, M.C., Jerrett, M., Pope, C.A., Krewski, D., Gapstur, S.M., Diver, W.R., Beckerman, B.S.,
604 Marshall, J.D., Su, J., Crouse, D.L., Burnett, R.T.: Long-Term Ozone Exposure and Mortality
605 in a Large Prospective Study, *Am. J. Respir. Crit. Care Med*, 193, 1134–1142,
606 <https://doi.org/10.1164/rccm.201508-1633OC>, 2016.
- 607 Van Der Werf, G.R., Randerson, J.T., Giglio, L., Van Leeuwen, T.T., Chen, Y., Rogers, B.M., Mu,
608 M., Van Marle, M.J.E., Morton, D.C., Collatz, G.J., Yokelson, R.J., Kasibhatla, P.S.: Global
609 fire emissions estimates during 1997–2016, *Earth Syst. Sci. Data*, 9, 697–720,
610 <https://doi.org/10.5194/essd-9-697-2017>, 2017.
- 611 Wang, N., Huang, X., Xu, J., Wang, T., Tan, Z., Ding, A.: Typhoon-boosted biogenic emission
612 aggravates cross-regional ozone pollution in China, *Sci. Adv.*, 8, eabl6166,
613 <https://doi.org/10.1126/sciadv.abl6166>, 2022.
- 614 Wang, P., Hui, P., Xue, D., & Tang, J.: Future projection of heat waves over China under global
615 warming within the CORDEX-EA-II project, *Clim. Dynam.*, 53(1–2), 957–973,
616 <https://doi.org/10.1007/s00382-019-04621-7>, 2019.
- 617 Wang, P., Tang, J., Wang, S., Dong, X., & Fang, J.: Regional heatwaves in china: a cluster analysis,
618 *Clim. Dynam.*, 50, 1901–1917, <https://doi.org/10.1007/s00382-017-3728-4>, 2018.
- 619 Wang, P., Yang, Y., Li, H., Chen, L., Dang, R., Xue, D., Li, B., Tang, J., Leung, L.R., Liao, H.: North



- 620 China Plain as a hot spot of ozone pollution exacerbated by extreme high temperatures,
621 Atmospheric Chem. Phys., 22, 4705–4719, <https://doi.org/10.5194/acp-22-4705-2022>, 2022.
- 622 Wang, P., Yang, Y., Xue, D., Qu, Y., Tang, J., Leung, L.R., Liao, H.: Increasing Compound Hazards
623 of Tropical Cyclones and Heatwaves over Southeastern Coast of China under Climate Warming,
624 J. Clim., 36, 2243–2257, <https://doi.org/10.1175/JCLI-D-22-0279.1>, 2023.
- 625 Wang, T., Xue, L., Brimblecombe, P., Lam, Y.F., Li, L., Zhang, L.: Ozone pollution in China: A
626 review of concentrations, meteorological influences, chemical precursors, and effects, Sci.
627 Total Environ., 575, 1582–1596, <https://doi.org/10.1016/j.scitotenv.2016.10.081>, 2017.
- 628 Wang, T., Zhong, Z., Sun, Y., Wang, J.: Impacts of tropical cyclones on the meridional movement
629 of the western Pacific subtropical high, Atmospheric Sci. Lett., 20, e893,
630 <https://doi.org/10.1002/asl.893>, 2019.
- 631 Wang, W., Zhou, W., Li, X., Wang, X., Wang, D.: Synoptic-scale characteristics and atmospheric
632 controls of summer heat waves in China, Clim. Dynam., 46, 2923–2941,
633 <https://doi.org/10.1007/s00382-015-2741-8>, 2016.
- 634 Wang, X., Chen, F., Wu, Z., Zhang, M., Tewari, M., Guenther, A., & Wiedinmyer, C.: Impacts of
635 weather conditions modified by urban expansion on surface ozone: Comparison between the
636 Pearl River Delta and Yangtze River Delta regions, Adv. Atmos. Sci., 26, 962–972,
637 <https://doi.org/10.1007/s00376-009-8001-2>, 2009.
- 638 Wang, Z., Hu, B., Zhang, C., Atkinson, P.M., Wang, Z., Xu, K., Chang, J., Fang, X., Jiang, Y., Shi,
639 Z.: How the Air Clean Plan and carbon mitigation measures co-benefited China in PM_{2.5}
640 reduction and health from 2014 to 2020, Environ. Int., 169, 107510



- 641 <https://doi.org/10.1016/j.envint.2022.107510>, 2022.
- 642 Wei, J., Li, Z., Li, K., Dickerson, R.R., Pinker, R.T., Wang, J., Liu, X., Sun, L., Xue, W., Cribb, M.:
- 643 Full-coverage mapping and spatiotemporal variations of ground-level ozone (O₃) pollution
- 644 from 2013 to 2020 across China, *Remote Sens. Environ.*, 270, 112775,
- 645 <https://doi.org/10.1016/j.rse.2021.112775>, 2022.
- 646 Wei, X., Lam, K. S., Cao, C., Li, H., & He, J.: Dynamics of the Typhoon Haitang Related High
- 647 Ozone Episode over Hong Kong, *Adv. Atmospheric Sci.*, 6089154,
- 648 <https://doi.org/10.1155/2016/6089154>, 2016.
- 649 Wu, J., Chen, Y., Liao, Z., Gao, X., Zhai, P., & Hu, Y.: Increasing risk from landfalling tropical
- 650 cyclone-heatwave compound events to coastal and inland China, *Environ. Res. Lett.*, 17(10),
- 651 105007, <https://doi.org/10.1088/1748-9326/ac9747>, 2022.
- 652 Xiao, Y.F., Duan, Z.D., Xiao, Y.Q., Ou, J.P., Chang, L., Li, Q.S.: Typhoon wind hazard analysis for
- 653 southeast China coastal regions, *Struct. Saf.*, 33, 286–295,
- 654 <https://doi.org/10.1016/j.strusafe.2011.04.003>, 2011.
- 655 Yang, Y., Li, M., Wang, H., Li, H., Wang, P., Li, K., Gao, M., Liao, H.: ENSO modulation of
- 656 summertime tropospheric ozone over China, *Environ. Res. Lett.*, 17, 034020,
- 657 <https://doi.org/10.1088/1748-9326/ac54cd>, 2022.
- 658 Yang, Y., Liao, H., Li, J.: Impacts of the East Asian summer monsoon on interannual variations of
- 659 summertime surface-layer ozone concentrations over China, *Atmospheric Chem. Phys.*, 14,
- 660 6867–6879, <https://doi.org/10.5194/acp-14-6867-2014>, 2014.
- 661 Yin, Z., Cao, B., Wang, H.: Dominant patterns of summer ozone pollution in eastern China and



- 662 associated atmospheric circulations, *Atmospheric Chem. Phys.*, 19, 13933–13943,
663 <https://doi.org/10.5194/acp-19-13933-2019>, 2019.
- 664 Ying, M., Zhang, W., Yu, H., Lu, X., Feng, J., Fan, Y., Zhu, Y., Chen, D.: An Overview of the China
665 Meteorological Administration Tropical Cyclone Database, *J. Atmospheric Ocean. Technol.*,
666 31, 287–301, <https://doi.org/10.1175/JTECH-D-12-00119.1>, 2014.
- 667 Zhan, C., & Xie, M.: Exploring the link between ozone pollution and stratospheric intrusion under
668 the influence of tropical cyclone Ampil, *Sci. Total Environ.*, 828, 154261,
669 <https://doi.org/10.1016/j.scitotenv.2022.154261>, 2022.
- 670 Zhan, C., Xie, M., Huang, C., Liu, J., Wang, T., Xu, M., Ma, C., Yu, J., Jiao, Y., Li, M., Li, S.,
671 Zhuang, B., Zhao, M., & Nie, D.: Ozone affected by a succession of four landfall typhoons in
672 the Yangtze River Delta, China: Major processes and health impacts, *Atmospheric Chem. Phys.*,
673 20(22), 13781–13799, <https://doi.org/10.5194/acp-20-13781-2020>, 2020.
- 674 Zhang, J., Gao, Y., Luo, K., Leung, L.R., Zhang, Y., Wang, K., Fan, J.: Impacts of compound extreme
675 weather events on ozone in the present and future, *Atmospheric Chem. Phys.*, 18, 9861–9877,
676 <https://doi.org/10.5194/acp-18-9861-2018>, 2018.
- 677 Zhang, M., Yang, Y., Zhan, C., Zong, L., Gul, C., & Wang, M.: Tropical cyclone-related heatwave
678 episodes in the Greater Bay Area, China: Synoptic patterns and urban-rural disparities. *Weather
679 and Climate Extremes*, 44, 100656. <https://doi.org/10.1016/j.wace.2024.100656>, 2024.
- 680 Zhang, Y., Dai, J., Li, Q., Chen, T., Mu, J., Brasseur, G., Wang, T., Xue, L.: Biogenic volatile organic
681 compounds enhance ozone production and complicate control efforts: Insights from long-term
682 observations in Hong Kong, *Atmos. Environ.*, 309, 119917,



683 <https://doi.org/10.1016/j.atmosenv.2023.119917>, 2023.

684 Zhou, Y., Yang, Y., Wang, H., Wang, J., Li, M., Li, H., Wang, P., Zhu, J., Li, K., Liao, H.: Summer

685 ozone pollution in China affected by the intensity of Asian monsoon systems, *Sci. Total*

686 *Environ.*, 849, 157785, <https://doi.org/10.1016/j.scitotenv.2022.157785>, 2022.

687



688 **Table 1.** Observed and simulated averaged surface MDA8 ozone ($\mu\text{g}/\text{m}^3$) in the Yangtze River Delta
 689 (YRD, 118—122° E, 30—33° N) and the Pearl River Delta (PRD, 110—115.5° E, 21.5—24° N)
 690 during TC-HDs and AHDs, as well as their differences (TC-HDs minus AHDs).

	YRD		PRD	
	Observed	Simulated	Observed	Simulated
TC-HDs	134.71	177.17	97.93	123.91
AHDs	147.92	199.11	91.13	116.91
Differences	-13.21	-21.94	6.8	7

691
 692 **Table 2.** Contributions of difference processes for the anomalous ozone mass ($\text{Gg O}_3/\text{day}$) from
 693 surface to 500 hPa for TC-HDs and AHDs relative to the summer climatology and their difference
 694 (TC-HDs minus AHDs) for YRD.

	Net chemical production	Vertical advection	Horizontal advection	Mixing
TC-HDs	1.70	0.03	-2.18	0.004
AHDs	0.46	-0.04	-1.03	-0.12
Differences	1.24	0.07	-1.15	0.12

695

696

697

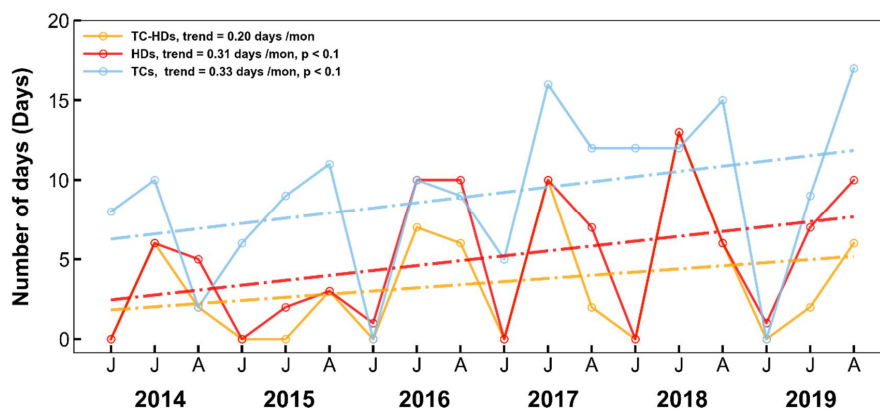


698 **Table 3.** Contributions of difference processes for the anomalous ozone mass ($\text{Gg O}_3/\text{day}$) from
699 surface to 500 hPa for TC-HDs and AHDs relative to the summer climatology and their difference
700 (TC-HDs minus AHDs) for PRD.

	Net chemical production	Vertical advection	Horizontal advection	Mixing
TC-HDs	0.21	-0.13	0.97	-0.002
AHDs	0.06	0.09	-0.84	-0.05
Differences	0.15	-0.22	1.81	0.05

701

702

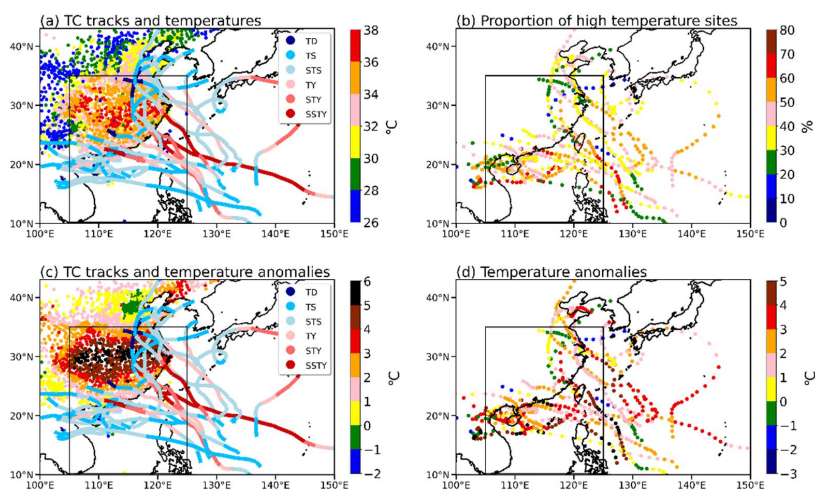


703

704 **Figure 1.** Monthly variations of the number of days of TC-HDs, total HDs, and total TCs during the

705 summer season (June, July and August) from 2014—2019.

706



707

708 **Figure 2.** Spatial characteristics of TC-HDs. (a) The distribution of average Tmax and TC tracks

709 during TC-HDs. (b) The proportion of high temperature sites over land region of SECC along with

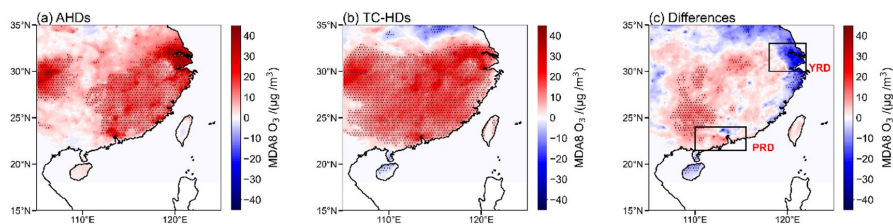
710 the movements of the TCs. (c) Average Tmax anomalies during TC-HDs period relative to the

711 summer climatology, along with the TC tracks categorized by different intensities. (d) Average

712 Tmax anomalies over land regions relative to the summer climatology, along with the movements

713 of TCs movement. SECC regions are outlined in red boxes in each panel.

714



715

716 **Figure 3.** The spatial distribution of surface MDA8 ozone concentration anomalies during the

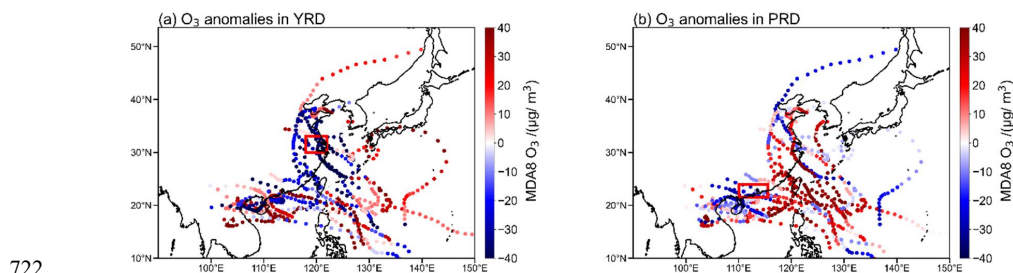
717 periods of (a) AHDs, (b) TC-HDs relative to the summertime climatology, as well as (c) their

718 difference (TC-HDs minus AHDs). Stippling regions indicate ozone anomalies that are significantly

719 difference from zero at the 95% confidence level. YRD and PRD regions are outlined in black boxes

720 in panel c.

721



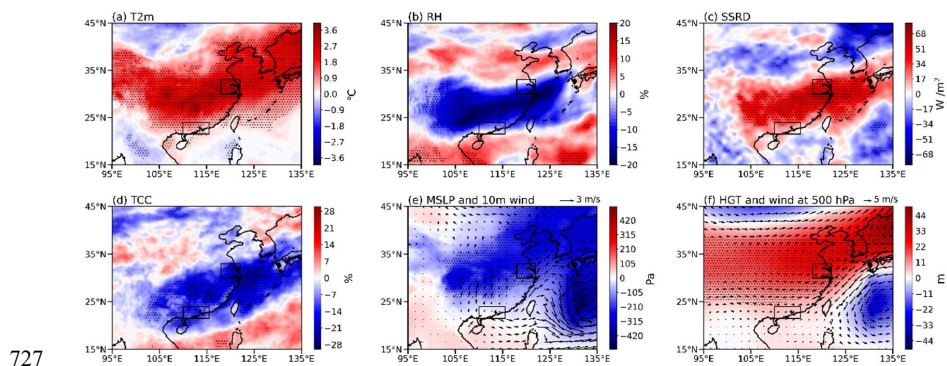
722

723 **Figure 4.** The average anomalies of surface MDA8 ozone concentrations over land regions of SECC

724 along with the movements of TCs associated with TC-HDs for (a) YRD and (b) PRD regions. YRD

725 (a) and PRD (b) regions are outlined in red boxes in panel (a) or (b).

726



727

728 **Figure 5.** The spatial distribution for the composites anomalies of (a) air temperature at 2m (T2m),

729 (b) relative humidity (RH), (c) surface solar radiation downwards (SSRD), (d) total cloud cover

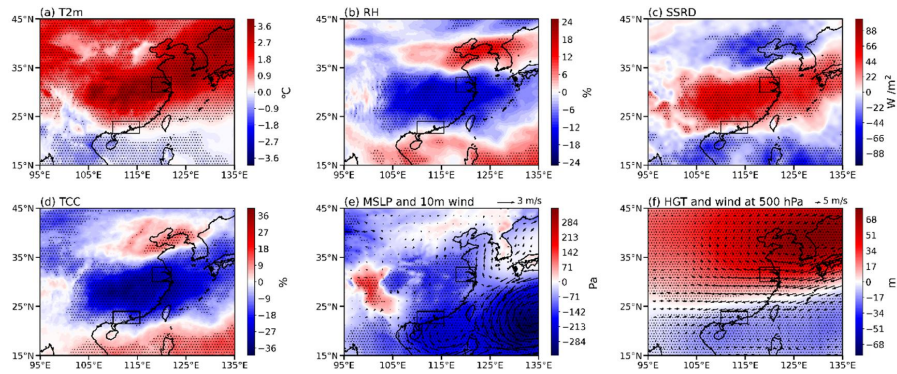
730 (TCC), (e) mean surface level pressure (MSLP) and 10-meter winds, and (f) geopotential height

731 (HGT) and winds at 500hPa during AHDs relative to the summer climatology. Stippling indicates

732 statistically significant anomalies above 95% confidence level. YRD and PRD regions are outlined

733 in black boxes in each panel.

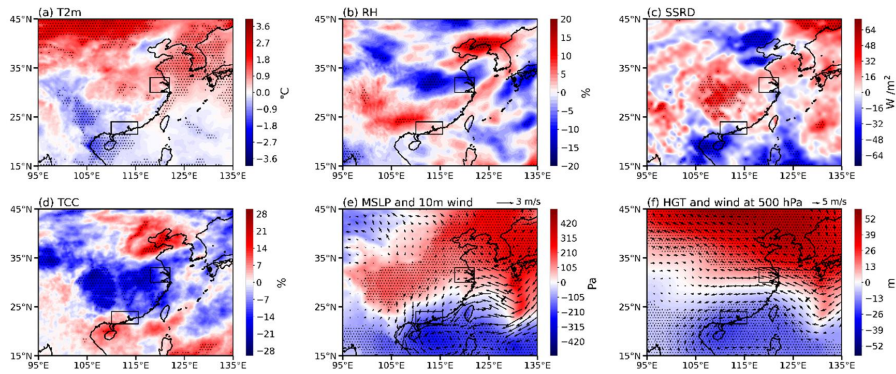
734



735

736 **Figure 6.** Same as in Figure 5, but for the anomalous meteorological conditions during TC-HDs.

737

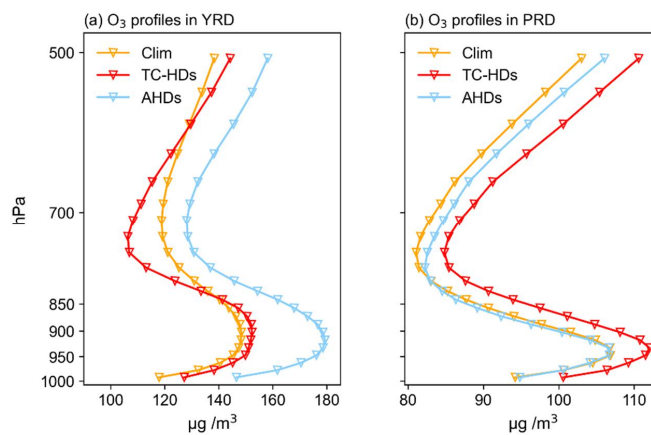


738

739 **Figure 7.** Same as in Figure 5, but for the differences between TC-HDs and AHDs (TC-HDs minus

740 AHDs).

741



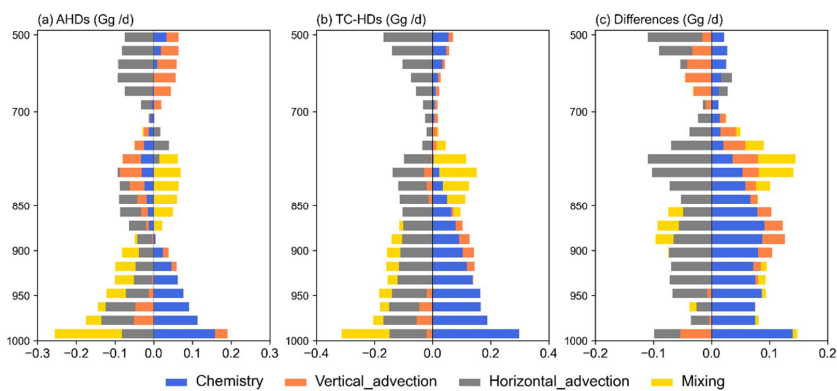
742

743 **Figure 8.** Vertical profiles of simulated daily ozone concentrations ($\mu\text{g}/\text{m}^3$) averaged over land

744 regions of SECC for TC-HDs, AHDs and for the summertime climatology (Clim) during 2014—

745 2019 for (a) YRD and (b) PRD.

746



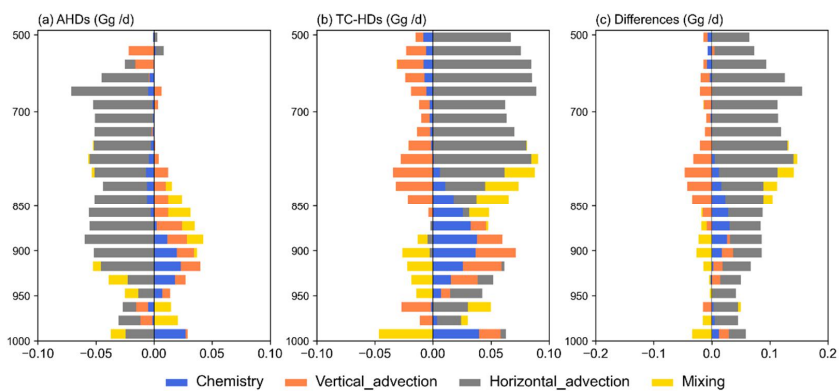
747

748 **Figure 9.** Vertical profiles of net changes in ozone mass (Gg O₃/day) anomalies averaged for YRD

749 for each process during (a) AHDs relative to summertime climatology, (b) TC-HDs relative to

750 summertime climatology average and their difference (TC-HDs minus AHDs).

751



752

753 **Figure 10.** Same as in Figure 9, but for the vertical profiles of net changes in ozone mass (Gg O₃/day)

754 anomalies averaged for PRD for each process.